PFAS Transport under Lower Water-Saturation Conditions Characterized with Instrumented-Column Systems

Matthew Bigler, Xuexiang He, and Mark L. Brusseau*

Environmental Science Department
The University of Arizona
Tucson, AZ, 85721

Submitted for review to:

Water Research

March 6, 2024

Revised: May 20, 2024

^{*}Corresponding author, Brusseau@arizona.edu

Abstract

1

2

3

4

5

6

7

8

9

10

11

12

13

14

15

16

17

18

19

20

21

22

23

The transport of PFOS and PFOA in well-characterized sand was investigated for relatively low water saturations. An instrumented column was used for some experiments to provide realtime in-situ monitoring of water saturation and matric potential. The results showed that water saturations and matric potentials varied minimally during the experiments. Flow rates were monitored continuously and were essentially constant. These results demonstrate that surfactantinduced flow and other nonideal hydraulic processes did not materially impact PFAS transport for the experiment conditions. Air-water interfacial adsorption was demonstrated to provide the great majority of retention for PFOS and PFOA. Retention was significantly greater at the lower water saturations (0.35-0.45) compared to the higher saturations (~0.66) for both PFAS, due to the larger extant air-water interfacial areas. Retardation factors were 5 and 3-times greater at the lower water saturations for PFOS and PFOA, respectively. Early breakthrough was observed for the PFAS but not for the non-reactive tracers at the lower water saturations, indicating the possibility that airwater interfacial adsorption was rate-limited to some degree. Independently determined retention parameters were used to predict retardation factors for PFOS and PFOA, which were similar to the measured values in all cases. The consistency between the predicted and measured values indicates that PFAS retention was accurately represented. In addition, air-water interfacial adsorption coefficients measured from the transport experiments were consistent with independently measured equilibrium-based values. Based on these results, it appears that the air-water interfacial adsorption processes mediating the magnitude of PFOS and PFOA retention under lower watersaturation conditions are consistent with those for higher water saturations. This provides some confidence that our understanding of PFAS retention obtained from work conducted at higher water saturations is applicable to lower water saturations.

Keywords: PFOS, PFOA, air-water interfacial adsorption, retention

1. Introduction

It is now well established that per and poly-fluoroalkyl substances (PFAS) are present in soils at numerous sites across the globe (e.g., Rankin et al., 2016; Washington et al., 2019; Brusseau et al., 2020a). The potential for PFAS to leach through the vadose zone and impact groundwater is a primary concern for these sites. As a result, the processes and factors influencing PFAS retention and migration in the vadose zone have been a focus of recent research. These investigations have included bench-scale transport experiments, field-characterization studies, and the application of conceptual and mathematical models. All three approaches are critical to developing a thorough understanding of PFAS transport in the vadose zone.

Among the different approaches, bench-scale miscible-displacement (i.e., "column") transport experiments serve as a means to directly examine under controlled conditions specific processes and factors mediating PFAS retention and transport. Initial such experiments for PFAS were conducted by Brusseau and colleagues (Lyu et al., 2018; Brusseau et al., 2019a), who demonstrated that retention under unsaturated-flow conditions is greater than under saturated conditions due to PFAS adsorption at air-water interfaces. They have since investigated the impact of porous-medium type, solution properties, PFAS chain length, mass-transfer processes, and the presence of PFAS mixtures and hydrocarbon surfactant on PFAS transport under unsaturated conditions (Brusseau, 2020; Lyu and Brusseau, 2020; Yan et al., 2020; Brusseau et al., 2021; Ji et al., 2021; Huang et al., 2022; Lyu et al., 2022a). Sun and colleagues have investigated the impact of porous-medium type, solution ionic composition, and the presence of hydrocarbon surfactant

specifically on perfluorooctanoic acid (PFOA) transport under unsaturated conditions (Lyu et al., 2020; Li et al., 2021; Lyu et al., 2022b). Abraham et al. (2022) have recently investigated the impact of trapped air bubbles on PFAS transport in porous media.

These works have contributed significantly to our understanding of PFAS retention and transport in unsaturated porous media. However, the great majority of the prior experiments were conducted using comparatively high water saturations, in the range of approximately 0.64 to 0.84. Field studies of infiltration and recharge have shown that water saturations are typically lower, even during active infiltration and drainage, ranging between approximately 0.2 to 0.6 (e.g., Yao et al., 2004; Rimon et al., 2007; Turkeltaub et al., 2014). These ranges are supported by mathematical-modeling simulations of PFAS vadose-zone transport, wherein the simulated water saturations remained between 0.2 and 0.6, depending upon the recharge rate and soil properties (Guo et al., 2020; Brusseau and Guo, 2022). A recent field study of PFAS distribution in porewater versus soil also reported water saturations ranging between 0.25 and ~0.6 (Schaefer et al., 2022a). Of course, the magnitude and range of values will depend on soil properties and site conditions. To our knowledge, only two sets of PFAS transport experiments have been conducted using lower saturations. Lyu et al. (2018) conducted an experiment at a water saturation of 0.35, whereas Lyu et al. (2020) conducted experiments at a water saturation of 0.45.

Decades of research have established that solute transport in macroscopically homogeneous porous media is often more complex under unsaturated conditions than for saturated conditions, wherein for example early breakthrough, extended concentration tailing, and increased spreading or dispersion are often observed. Such behavior is typically attributed to greater flow-path tortuosity, greater variances in porewater velocities, and the presence of stagnant/immobile water under unsaturated conditions. Numerous bench-scale solute-transport experiments have

demonstrated that this nonideal behavior is a function of water saturation, with greater nonideality often observed at lower water saturations (e.g., Biggar and Nielsen, 1960; Krupp and Elrick, 1968; Gaudet et al., 1977; De Smedt and Wierenga, 1984; Bond and Wierenga, 1990; Padilla et al., 1999; Toride et al., 2003; Kumahor et al., 2015; Zhuang et al., 2021). This is also supported by the results of pore-scale modeling and imaging studies (e.g., Raoof and Hassanizadeh, 2013; Hasan et al., 2020).

While the noted research has focused on nonreactive solutes, the retention and transport of interfacially active solutes such as PFAS will also be affected by these processes. However, their transport may in addition be impacted by changes in accessibility to air-water interfaces accruing to changes in water saturation. Access to air-water interfaces for solutes migrating in the aqueous phase typically becomes more constrained as water saturation decreases (e.g., Costanza-Robinson and Brusseau, 2002; Brusseau et al., 2007). This can lead to an increase in mass-transfer constraints affecting air-water interfacial adsorption, which in turn can impact retention and transport behavior (Brusseau, 2020). Such behavior for example has been speculated to result in the underestimation of PFAS air-water interfacial adsorption coefficients (Schaefer et al., 2022b).

The monitoring of water saturations in all of the prior works was done gravimetrically by weighing the columns. While this approach produces accurate measurements of column-averaged values, it does not provide information on the internal distribution of water saturation. Some investigators have speculated that uncertainty in the distribution or status of water saturation may have resulted in errors in quantifying the retention behavior of hydrocarbon surfactants (Costanza-Robinson and Henry, 2017) or PFAS (Schaefer et al., 2022b) in transport studies. Furthermore, the occurrence of surfactant-induced flow is a potential concern for unsaturated-flow experiments conducted with interfacially active solutes (e.g., Kim et al., 1997; Smith and Gillham, 1999;

Karagunduz et al., 2015; Costanza-Robinson and Henry, 2017). These issues can be addressed by employing an instrumented-column system to provide real-time in-situ monitoring of water saturation and matric potential. Such highly instrumented columns have been used successfully for example to investigate the transport of butanol (e.g., Smith and Gillham, 1999) and silica colloids (Lenhart and Saiers, 2002) under unsaturated-flow conditions.

Based on the preceding discussion, it is possible that PFAS retention and transport may be subject to greater nonideal behavior at the lower water saturations that are representative of typical field conditions. Hence, additional investigations of PFAS transport under lower water-saturation conditions are clearly warranted. Additionally, the use of an instrumented-column system would enhance the investigation. The objective of this study is to examine the transport of PFAS under relatively low water saturations. Miscible-displacement experiments are conducted for perfluorooctanesulfonic acid (PFOS) and PFOA transport in a well-characterized sand that has been used in prior experiments, allowing direct comparative analysis. An instrumented column that is equipped with multiple amplitude domain reflectometry (ADR) probes and tensiometers/pressure-transducers is employed for select experiments to provide real-time in-situ monitoring of water saturation and matric potential. To our knowledge, this represents the first time that such a system has been used to investigate PFAS transport. Independently determined values for retention parameters are used to predict retardation factors, which are subsequently compared to the measured values. These experiments help to fill in the gap examining the impact of lower water saturations on the retention and transport of PFAS in unsaturated media.

115

95

96

97

98

99

100

101

102

103

104

105

106

107

108

109

110

111

112

113

114

116

2. Materials and methods

2.1 Materials

118

119

120

121

122

123

124

125

126

127

128

129

130

131

132

133

134

135

136

137

138

139

140

The experiments were conducted with PFOS (CAS# 1763-23-1, Sigma-Aldrich, 98%) and PFOA (CAS# 335-67-1, AIKE Reagent, 98%) as the representative PFAS. Input concentrations (C₀) of 100 μg/L were used for both to be consistent with our prior experiments. Pentafluorobenzoic acid (PBA, 120 mg/L), which is not a PFAS, and sodium bromide (0.01 M) were used as the nonreactive tracers (NRTs). Sodium dodecyl benzene sulfonate (SDBS, 35 mg/L) was used as the air-water interfacial adsorptive tracer. A background electrolyte (0.01 M NaCl) was used to maintain a constant ionic strength for all experiments. Surface tensions of the tracer solutions were measured with a force tensiometer (Sigma 70, Biolin Scientific) using the Du Nuoy ring method. No measurable difference in surface tension was observed between 0.01 M NaCl and 0.01 M NaBr solutions. All aqueous solutions were prepared in deionized water (\geq 18.2 M Ω •cm resistivity) from a NANOpure ultrapure water system (Barnstead®). The porous medium used for these experiments is 40/50 mesh quartz sand (Accusand). This sand has been thoroughly characterized in previous studies including measurements of the soil water characteristic (Brusseau and Guo, 2021), air-water interfacial area (Araujo et al., 2015; Brusseau et al. 2015; Brusseau et al., 2020b; El Ouni et al. 2021), and solid-phase sorption for PFOS and PFOA (Van Glubt et al., 2021). The medium has low organic-carbon (0.04%) and metaloxide (0.003%) contents, and no clay minerals. This medium has a low sorption capacity for PFOS and PFOA (Van Glubt et al., 2021), which supports a focus on the contributions of air-water interfacial adsorption to retention. Three column setups were used for the experiments. One setup employed a standard solidbarrel column, which was 15 cm long with an internal diameter of 2.5 cm. The second setup

comprised a stacked set of segmented rings of 1.5 cm height and 2.8 cm diameter (see Figure 1). Silicone tape was wrapped around the stacked rings to hold them in place and ensure they were water-tight during the experiment. This segmented-column design facilitates the measurement of water saturation at discrete intervals along the length of the column at the end of an experiment. Ten-micron polypropylene porous plates (Scientific Commodities, BB2062-10BL) were placed at the bottom of both columns. The top caps were removed during unsaturated-flow experiments to allow equilibration with the atmosphere. Water saturation was monitored gravimetrically for these two setups by weighing both the column and the effluent samples.

The third setup employed an instrumented column (Figure 1), 30 cm long with an internal diameter of 12.17 cm. The larger diameter was required to accommodate the instrumentation. Three intervals of instrument suites were installed at heights of 5, 15, and 25 cm. Each of these suites contained a tensiometer/pressure transducer couple (rods from SoilMoisture Equipment and transducers GT3-30 from ICT International) to measure matric potential and an ADR probe (ICT international MP306) to measure water saturation. Care was taken to ensure that the instruments within each layer occupied the same horizontal plane. The top of the column has four ports. Three of the ports were used to inject the influent aqueous solutions through a porous frit to ensure uniform distribution across the column cross section. The fourth is closed for saturated-flow experiments, and open for unsaturated-flow experiments to ensure pressure equilibration across the column. The bottom has three effluent ports and a 10-micron polypropylene porous plate (Scientific Commodities, BB2062-10AL) to retain the media and ensure uniform pressure distribution. Given the comparative large size of this system, it was used for select experiments to minimize generation of PFAS waste.

An HPLC piston pump (Shimadzu LC20 AD) was used to inject the solutions into the column at a constant specific discharge of either 0.05 or 0.09 cm/min. One of two vacuum systems was used to generate unsaturated flow. One system employed a set of vacuum flasks and a vacuum pump (Figure 1), while the other employed a custom-built vacuum chamber and pump.

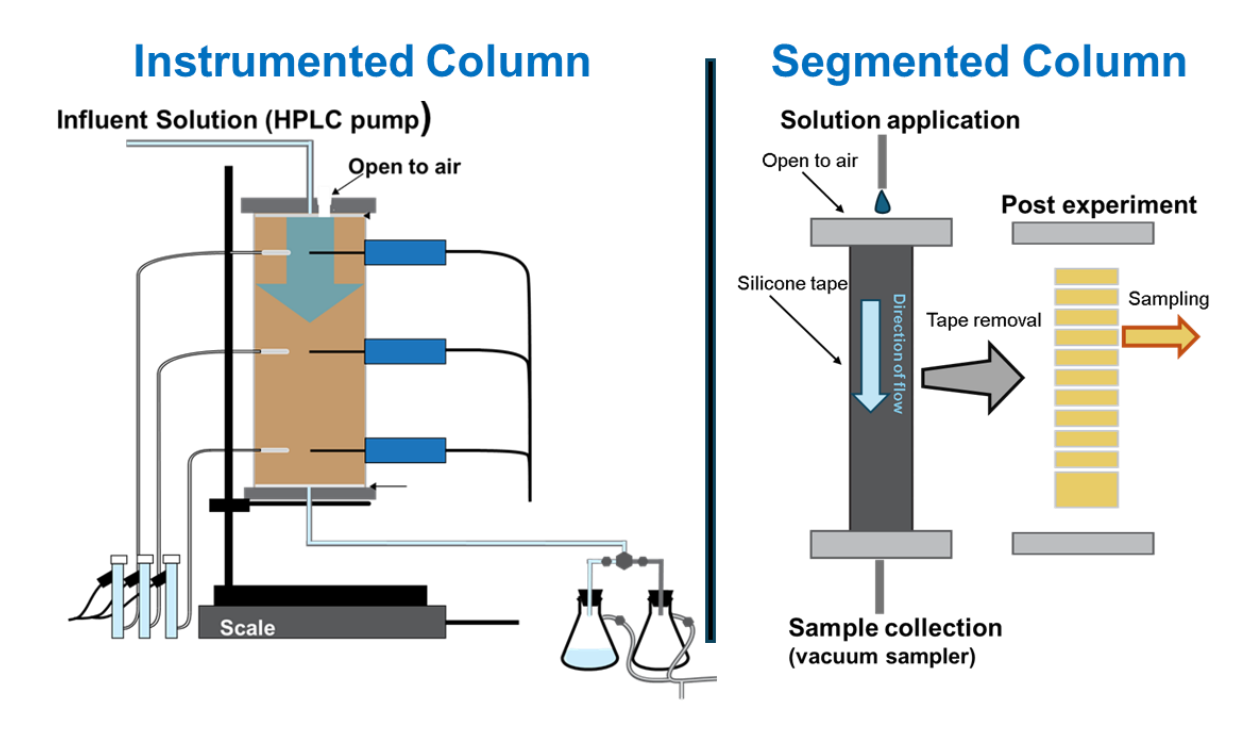


Figure 1. Diagrams of the instrumented-column and segmented-column setups.

2.2 Methods

Multiple sets of experiments were conducted for this study. (1) The soil water characteristic (SWC) was measured in-situ by monitoring the tensiometers and ADRs in the instrumented column during primary drainage. These in-situ measurements will be compared to new and previous measurements conducted using a standard Tempe-cell method. (2) Nonreactive tracer tests were conducted to characterize the influence of hydraulic properties on water flow and solute transport. (3) Interfacial tracer tests were conducted to obtain independent measures of air-water

interfacial area at the water saturations used for the PFAS experiments. These data supplement the numerous prior measurements that have been reported for this medium. (4) PFOS and PFOA transport was investigated individually to examine the impact of air-water interfacial adsorption on retention under lower water-saturation conditions. (5) Initial experiments were conducted to characterize the potential impact of PFAS presence on spatial and temporal water-saturation distributions and tracer transport. One experiment was conducted with the instrumented column using an influent PFOS concentration of 10 mg/L, 100-times larger than that used for the primary experiments, to characterize the potential impact of surfactant-induced flow. Another experiment was conducted with the segmented column and a PFOS concentration of 1 mg/L to measure water saturation at discrete intervals along the length of the column. Finally, a preliminary experiment was conducted to test the simultaneous application of the NRT and PFOS (0.1 mg/L).

Measurements of the SWC: Simultaneous monitoring of water saturation and matric potential during drainage in the instrumented column provides a direct, in-situ measure of the SWC. These data are compared to prior and new measurements conducted with the standard Tempe-cell method. For the Tempe-cell measurements, each standard 6-cm Tempe cell (Soilmoisture 1400B01M1-6) was dry packed to the target bulk density. Porous 1-bar ceramic plates were pre-saturated with solution and attached to the cells. The Tempe cells were then slowly saturated with degassed 0.01 M NaCl solution. Once saturated, drainage was induced by a regulated pressure source and saturation was determined gravimetrically (ASTM, 2016). The prior Tempe-cell measurements were reported in Brusseau and Guo (2021).

Preparation and operation of the packed columns: Each column was packed with air-dried media to bulk densities of approximately 1.69 to 1.73 g/cm³ and porosities of approximately 0.30 to 0.35. The column was then saturated with degassed 0.01 M NaCl solution, introduced from the

bottom of the column. The mass of the column was monitored gravimetrically, and a stable mass was used to indicate full saturation. This was confirmed via ADR measurements for the instrumented column.

Once the column was saturated, the influent flow was switched to the top of the column. The top cap was removed for the standard and segmented columns to allow equilibration with the atmosphere. The vent at the top of the column was opened for the instrumented column. Steady unsaturated flow was achieved by modifying the bottom vacuum pressures and monitoring the influent and effluent flow rates. In addition, the ADRs and tensiometers were monitored within the instrumented column. Once steady-state flow was achieved, the respective transport experiments were initiated. The effluent samples were weighed to determine the effluent flow rates and to help monitor potential changes in water saturation within the column.

Effluent samples were collected from the bottom of the column. The effluent sample was delivered to the first of two flasks for the vacuum-flask system, and the flow was switched to the second flask when the desired sample volume was obtained. After the sample was collected, the first flask was cleaned, purged to the vacuum pressure of the manifold, and reattached. The process was then repeated for the second flask. This process ensured minimal fluctuations in vacuum pressures throughout the duration of the experiment. Measurements conducted with a manometer connected to the system demonstrated that purging the flasks before reattachment to the vacuum system maintained an uninterrupted vacuum pressure on the bottom of the column. For the vacuum-chamber system, the samples were delivered to a fraction collector housed within the chamber. The effluent samples were analyzed for the relevant solutes as described in the next section. For the segmented column, the tape was removed at the completion of the experiment and the soil from each ring was weighed, dried, and weighed again to determine water saturation.

Tracer and PFAS transport experiments: Experiments were conducted to characterize transport of PFOS, PFOA, SDBS, and the nonreactive tracers. An overview is presented in Table 1. The PFOS and PFOA transport experiments were conducted in duplicate, while the SDBS tests were conducted in triplicate. For most experiments, an NRT test was conducted first, followed by PFOS, PFOA, or SDBS transport. In select cases, the NRT test was conducted simultaneously with the PFAS or SDBS transport. For the SDBS experiment, two NRT tests were conducted using the same packed column, one sequentially with PBA and bromide present and one simultaneously with bromide. When bromide was used as the NRT, the NaCl solution was replaced with NaBr, such that the ionic strength was not altered.

 Table 1. Overview of Transport Experiments

Experiment	Column Type	Notes	
SDBS-1	Instrumented	NRT-sequential	
SDBS-2	Instrumented	NRT-sequential	
SDBS-3	Instrumented	NRT-sequential & simultaneous	
PFOS-initial	Instrumented	Test water-saturation and matric-potential measurements	
PFOS-initial	Segmented	Test water-saturation spatial distribution	
PFOS-initial	Standard	Test simultaneous NRT	
PFOS-1	Segmented	NRT-sequential	
PFOS-2	Standard	NRT-sequential	
PFOA-1	Instrumented	NRT-sequential	
PFOA-2	Standard	NRT-simultaneous	

The experiments were conducted for a target nominal water saturation of 0.35 for PFOA and 0.45 for PFOS. These saturations represent the mid-range of those reported for the field and modeling studies cited in the Introduction. The larger water saturation was used for PFOS to reduce the magnitude of retardation and the requisite experiment timeframe. The specific water saturations were measured for each experiment and are reported in Table 2. The results of these experiments will be compared to the results of prior experiments conducted at higher water saturations (Brusseau et al., 2021; Huang et al., 2022). These prior studies used the same porous medium and input concentrations.

2.3 Chemical analysis

Pentafluorobenzoic acid (254 nm wavelength) and SDBS (223 nm wavelength) concentrations were measured by UV-vis spectrophotometry. Bromide concentrations were determined using a bromide ion selective electrode (Thermo Scientific 9635BNWP). PFOS and PFOA were analyzed at the University of Arizona WEST Center by liquid chromatography tandem mass spectrometry (LC-MS/MS), with an Agilent 1290 Infinity HPLC coupled with an Agilent 6460 Triple Quadrupole LC/MS. Chromatographic separation was achieved using a Phonomenex Gemini C18 column (100 x 3 mm, 3 μm), which was paired with a Phonomenex Guard column (50 x 3 mm, 3 μm) and maintained at a temperature of 40°C. The mobile phase consisted of 20 mM ammonium acetate (Sigma Millipore) and 99.8+% HPLC Grade methanol (Thermo Scientific). The MS was operated in negative ion mode, with the collision energy set to 54 eV for PFOS and 8 eV for PFOA. Standard QA/QC procedures were employed, including periodical spikes of the blank and standards. Data were collected by Agilent MassHunter and analyzed by

Skyline (MacLean et al., 2010). The method detection limits (MDLs) calculated according to EPA revision 2 (EPA, 2016) are approximately 40 ng/L in 0.01 M NaCl solution.

2.4 Data analysis

Breakthrough curves were developed by plotting relative concentrations versus eluted pore volumes. The concentration measured for each sample was divided by the input concentration to determine relative concentrations. The volume of solution displaced from the column was divided by the volume of solution retained by the column under the extant water saturation to determine pore volumes. Retardation factors were determined by moment analysis of the measured breakthrough curves, as detailed in prior works (Van Glubt et al., 2021). The total retention of PFAS or SDBS under unsaturated conditions is governed by adsorption at the air-water interface and adsorption at the solid-water interface. The retardation factor is defined as:

271
$$R = 1 + \frac{K_f C^{n-1} \rho_b}{\theta_w} + \frac{K_{aw} A_{aw}}{\theta_w}$$
 (1)

where ρ_b is the bulk density, K_f is the solid phase Freundlich sorption coefficient, n is the Freundlich parameter, C is the aqueous concentration of the input pulse, A_{aw} is the air-water interfacial area, and K_{aw} is the air-water interfacial adsorption coefficient. The fraction of retention associated with air-water interfacial adsorption (FAWIA) is calculated as:

276
$$FAWIA = [R - 1 - (\frac{K_f C^{n-1} \rho_b}{\theta_w})]/(R - 1)$$
 (2)

The measured retardation factors obtained from moment analysis of the breakthrough curves will be compared to predicted values determined using independent measures of the parameters comprising equation (1). The bulk density and volumetric water contents are measured for each experiment. The Freundlich solid-phase sorption parameters, K_f (PFOS-0.15, PFOA-0.1) and n (PFOS-0.81, PFOA-0.87), were determined in a prior study (Van Glubt et al., 2021). The

study used batch and column methods to measure isotherms for both PFOS and PFOA sorption by the sand used in the present study. The K_{aw} values (PFOS-0.034, PFOA-0.0027) were determined from surface-tension measurements reported in a prior study (Brusseau et al., 2021). The A_{aw} values were measured with the interfacial tracer tests conducted with SDBS. These measurements were corroborated with the prior measurements of interfacial area conducted for this sand (Araujo et al., 2015; Brusseau et al. 2015; Brusseau et al., 2020b; El Ouni et al. 2021).

Note that because values for A_{aw} are available from independent measurements, values for K_{aw} can be determined from the retardation factors measured with the transport experiments through solving equation (1). This approach will be used as another means of assessing the results of the experiments. The K_{aw} values determined with this approach will be compared to those determined from surface-tension measurements (reported above) as well as studies using aerosolgeneration and surface-microlayer sampling methods. For these latter two methods, the enrichment factors (EF) measured in the experiments can be converted to K_{aw} values through the following definition: $EF = 1 + (A/V) K_{aw}$, where A is the surface area of the interface and V is the volume of water comprising the water film (surface-microlayer sampling) or aerosol (aerosol generation).

As discussed in the Introduction, it is possible that the retention and transport of PFAS under unsaturated-flow conditions may be influenced by mass-transfer constraints. The impact of mass-transfer constraints during advective transport can be assessed through the use of Damkholer Numbers. This approach was used for example by Brusseau (2020) to evaluate the impact of rate-limited air-water interfacial adsorption on the retention and transport of PFAS and SDBS. The Damkholer Number represents in this case a comparison (ratio) of the hydraulic residence time and the characteristic time for mass transfer. It is assumed for the present analysis that air-water

interfacial adsorption is mediated by diffusive mass transfer to and from the air-water interfaces 305 (Brusseau, 2020).

The representative Damkohler Number (ω) for this case is given as:

$$\omega = \frac{aD_wL}{l^2v_w} \tag{3}$$

304

306

308

309

310

311

312

313

314

315

316

317

321

322

323

324

326

where a is a geometric shape factor (\sim 3 for planar geometry), D_w is the effective diffusion coefficient in porewater $[L^2/T]$, l is the characteristic diffusion length, L is the representative transport distance (column length), v_w is the mean linear porewater velocity $[v_w = q_w/\theta_w; L/T]$, and $q_w = \text{Darcy flux [L/T]}$. The effective diffusion coefficient is defined as $D_w = \theta_w D_{w0} \tau$, where D_{w0} is the diffusion coefficient in bulk water [L²/T] and τ is a tortuosity factor. The θ_w term accounts for the fraction of cross-sectional area of pore space available for diffusion and the tortuosity factor accounts for the complex diffusive paths associated with the pore network structure. Numerous expressions have been developed to determine tortuosity factors for soils. One of the most widely used expressions is that attributed to Millington and Quirk (1961), where $\tau = \theta_w^{7/3}/\theta_T^2$, and θ_T is porosity.

318 Based on equation (3), the ω values for two different water saturations can be compared 319 as:

$$\frac{\omega_2}{\omega_1} = \frac{D_{w2}}{D_{w1}} \frac{v_{w1}}{v_{w2}} \tag{4}$$

assuming the same shape factor, column length, and diffusive path length. The latter term may change as a function of water saturation, but will be assumed to be constant as a first approximation. Substituting in the definitions of D_w and v_w , and employing the Millington and Quirk representation of tortuosity, results in:

$$\frac{\omega_2}{\omega_1} = \frac{\theta_{w2}^{13/3}}{\theta_{w1}^{13/3}} \tag{5}$$

3. Results and discussion

3.1 Characterization of hydraulic and interfacial-area properties

The soil-water characteristic for the sand packed in the instrumented column was measured in-situ by monitoring matric potential and water saturation during drainage events that started from initial saturated conditions. These measurements are compared in Figure 2 to new and previous independent measurements conducted using the standard Tempe-cell method. The in-situ measurements match very well to the two sets of triplicate Tempe-cell measurements. These results demonstrate that the instruments produce accurate responses to and measurements of changes in water saturation and matric potential.

Water saturations were monitored with the ADR probes during a preliminary experiment conducted with a PFOS input concentration of 10 mg/L (Figure 3). Water saturation is observed to be similar among the three depths, very close to the targeted saturation of 0.45. The water saturations also exhibit minimal variation throughout the experiment, with coefficients of variation (COV) of ~0.1%. Similar results are observed for an experiment conducted with PFOA at a concentration of 0.1 mg/L. In addition, the matric potentials are observed to be relatively constant over the course of the experiments. These results demonstrate that conditions of steady unsaturated flow and uniform water saturation were attained for the experiments.

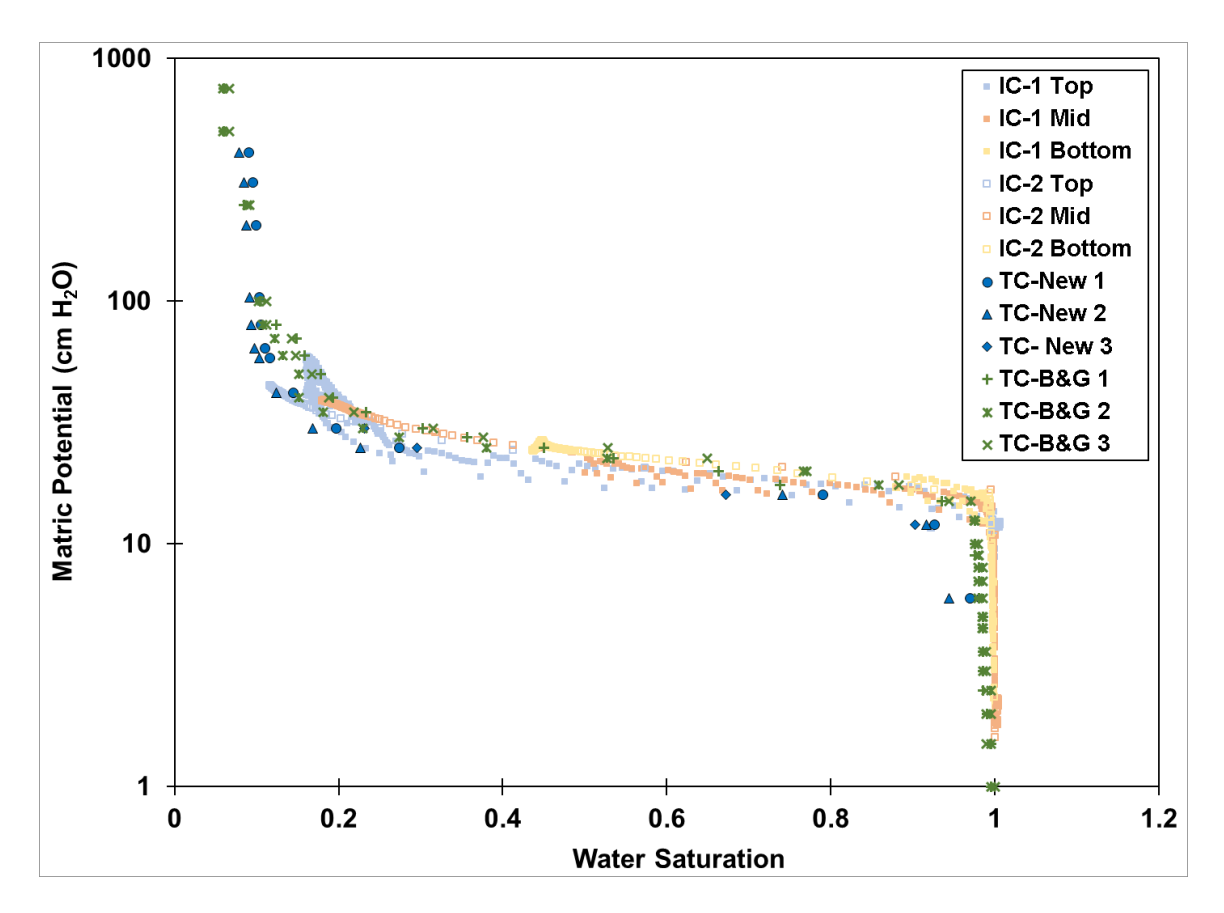


Figure 2. Measured soil water characteristic curves for the sand under primary drainage conditions. IC data sets represent measurements conducted in-situ for the instrumented column employing the ADR and tensiometer probes. IC-1 and IC-2 represent separate tests. TC data represent independent measurements obtained with the Tempe Cell method. The data designated as "New" represent new measurements conducted in the present study; those designated as "B&G" are from Brusseau and Guo, 2021.

The presence of surfactant in solution has the potential to cause surfactant-induced flow under unsaturated conditions, as discussed in the Introduction. The results presented in Figure 3 for the $C_0 = 10 \text{ mg/L}$ experiment indicate that there was minimal measurable impact of surfactant-induced flow accruing to the introduction of the PFAS solution. Given that the input concentration for that PFOS experiment is 100-times higher than the concentrations used for the primary experiments, it is reasonable to conclude that surfactant-induced flow is not a concern for the primary experiments. This is consistent with the results of the PFOA 0.1 mg/L experiment as well

as prior experiments and model simulations conducted at higher water saturations with similarly low input PFAS concentrations (Brusseau et al., 2020b, 2021; El Ouni et al., 2021).



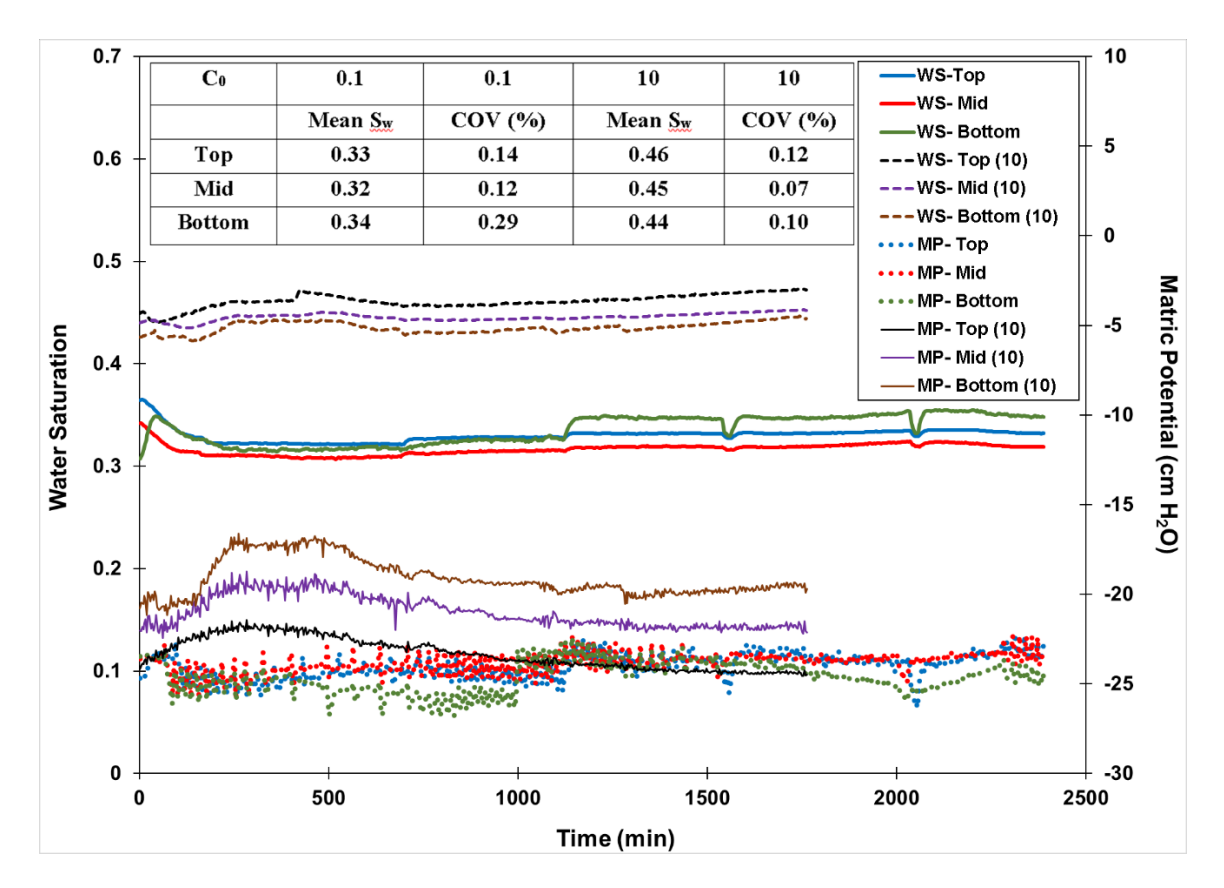
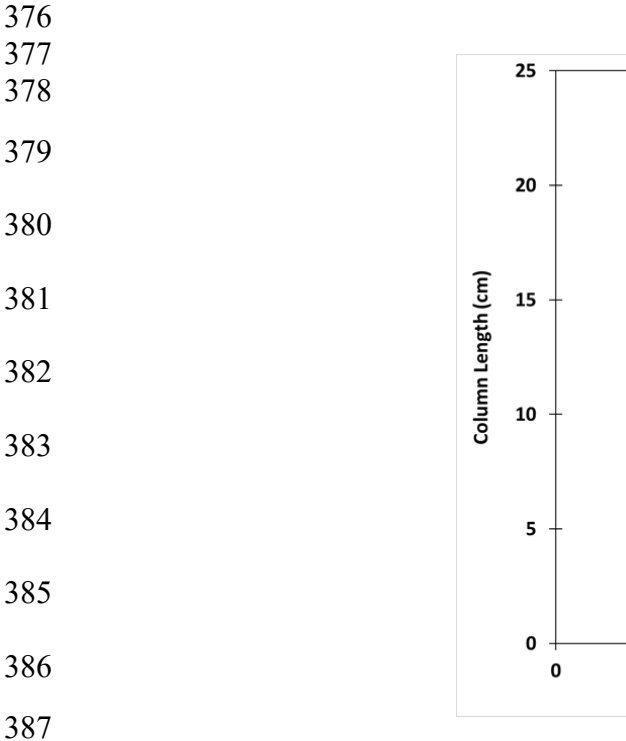


Figure 3. Measurements of water saturation (WS) and matric potential (MP) obtained for two experiments conducted with the instrumented column. Two input concentrations (C_0) were used: $C_0 = 10$ mg/L PFOS (noted in the legend as "(10)") and $C_0 = 0.1$ mg/L PFOA (no notation). Information on mean water saturations (S_w) and associated coefficients of variation (COV) are reported in the table inset.

The distribution of water saturation along the length of the column was measured in the experiments conducted with the segmented column (see Figure 4). The saturations are reasonably uniform, matching the prior discussed results. Finally, the mass of every effluent sample was measured during each experiment to monitor for potential changes in flow rate and associated water saturations. The masses varied by <1% for the present PFAS experiments (see Table 2). This indicates steady flow was maintained, consistent with the results presented in Figure 3.



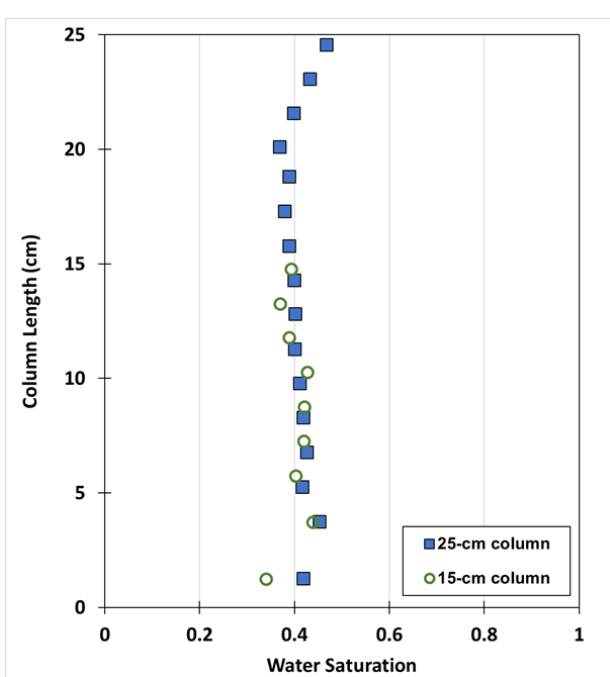


Figure 4. Water saturations measured along the length of segmented columns for PFOS $C_0 = 1$ (25-cm) and 0.1 (15-cm) mg/L experiments.

Representative breakthrough curves for the nonreactive tracers are presented in Figure 5. The breakthrough curves are very similar for the three types of columns, indicating that the column type has no impact on water flow and solute transport. The breakthrough curves are sharp and symmetrical, and measured retardation factors are 1. These results indicate conditions of uniform flow with no measurable impacts of potential non-advective flow domains on solute transport. Notably, the breakthrough curves for the simultaneous NRT-PFAS and NRT-SDBS experiments are coincident with the breakthrough curves measured for the sequential experiments. This demonstrates that the presence of PFAS or SDBS has no measurable impact on the advective-dispersive transport of the NRT, which indicates that PFAS or SDBS has no impact on water flow (including surfactant-induced flow). This is consistent with the hydraulic measurements discussed for Figure 3.

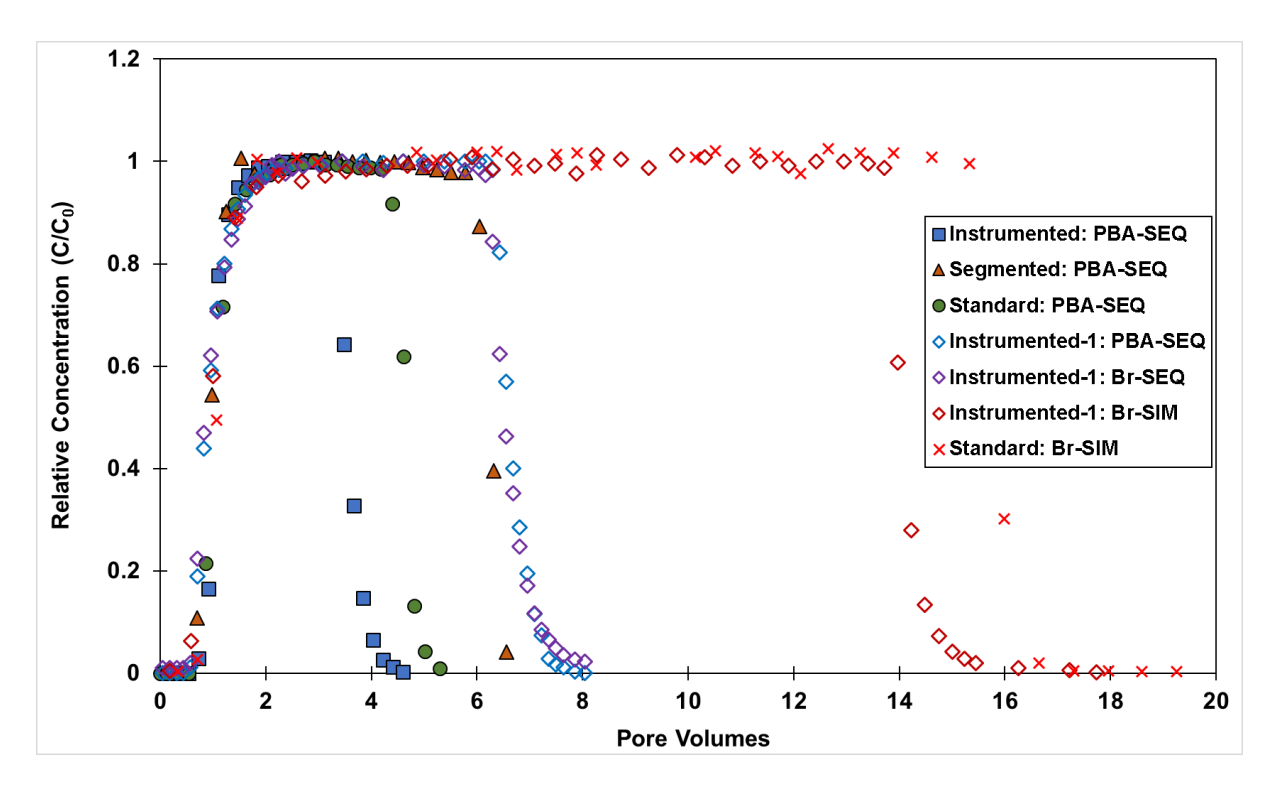


Figure 5. Breakthrough curves for transport of nonreactive tracers (NRT) under unsaturated-flow conditions (water saturation of 0.4 or 0.46). Note that the input-pulse size varied for each experiment. Representative data sets are presented for each of the three types of columns used in the experiments: Instrumented, Segmented, and Standard. PBA represents pentafluorobenzoic acid, Br represents bromide, SEQ means the NRT and PFAS/SDBS experiments were conducted separately, whereas SIM means they were conducted simultaneously. The "Instrumented-1" data represent results measured for the same packed column.

Interfacial tracer tests were conducted with SDBS to measure air-water interfacial area for the lower water saturations of these experiments. An illustrative breakthrough curve is presented in Figure 6. The mean air-water interfacial area determined from three experiments conducted at a water saturation of 0.39 is 283 (±19) cm⁻¹, with a COV of 6.6%. The measurement variability is quite low, especially considering that the three experiments were conducted using separate packed columns. Numerous prior interfacial tracer tests have been conducted for this sand using a range of methods (Brusseau, 2023). An empirical function was determined for these data that allows interpolation of interfacial areas for a given water saturation. The measured areas obtained from

the experiments conducted in the present study are consistent with the value (259 \pm 18 cm⁻¹) determined from the function for the given water saturation, with overlapping uncertainty intervals.

3.2 PFAS transport

Breakthrough curves for PFOS and PFOA transport are presented in Figure 6. Results of the present experiments conducted at lower water saturations are compared to those from prior studies conducted at higher saturations. Notably, greater retardation of both PFOS and PFOA is observed for the breakthrough curves measured at the lower water saturations. This is consistent with what would be anticipated due to the greater magnitudes of air-water interfacial area present at the lower water saturations. Greater retardation is observed for PFOS compared to PFOA for both sets of water saturations. This is expected given the greater interfacial activity of PFOS and its correspondingly larger air-water interfacial adsorption coefficient.

Table 2. Results for PFAS transport experiments.

PFAS	Water Saturation	R Measured	R Predicted	FAWIA ^a	Q COV ^b (%)
PFOS-1	0.46	59.5	55.0	0.94	0.3
PFOS-2	0.46	45.8	45.6	0.94	0.6
PFOS	0.68	10.2	10.6	0.84	1.4
PFOS	0.65	11.0	13.0	0.86	0.2
PFOA-1	0.35	9.9	10.2	0.76	0.5
PFOA-2	0.35	9.2	9.2	0.77	0.9
PFOA	0.66	3.0	2.9	0.61	4.7
PFOA	0.68	3.1	2.8	0.63	4.4

^aFraction of retention associated with air-water interfacial adsorption

^bCoefficient of variation of flow rate as determined from masses of every effluent sample

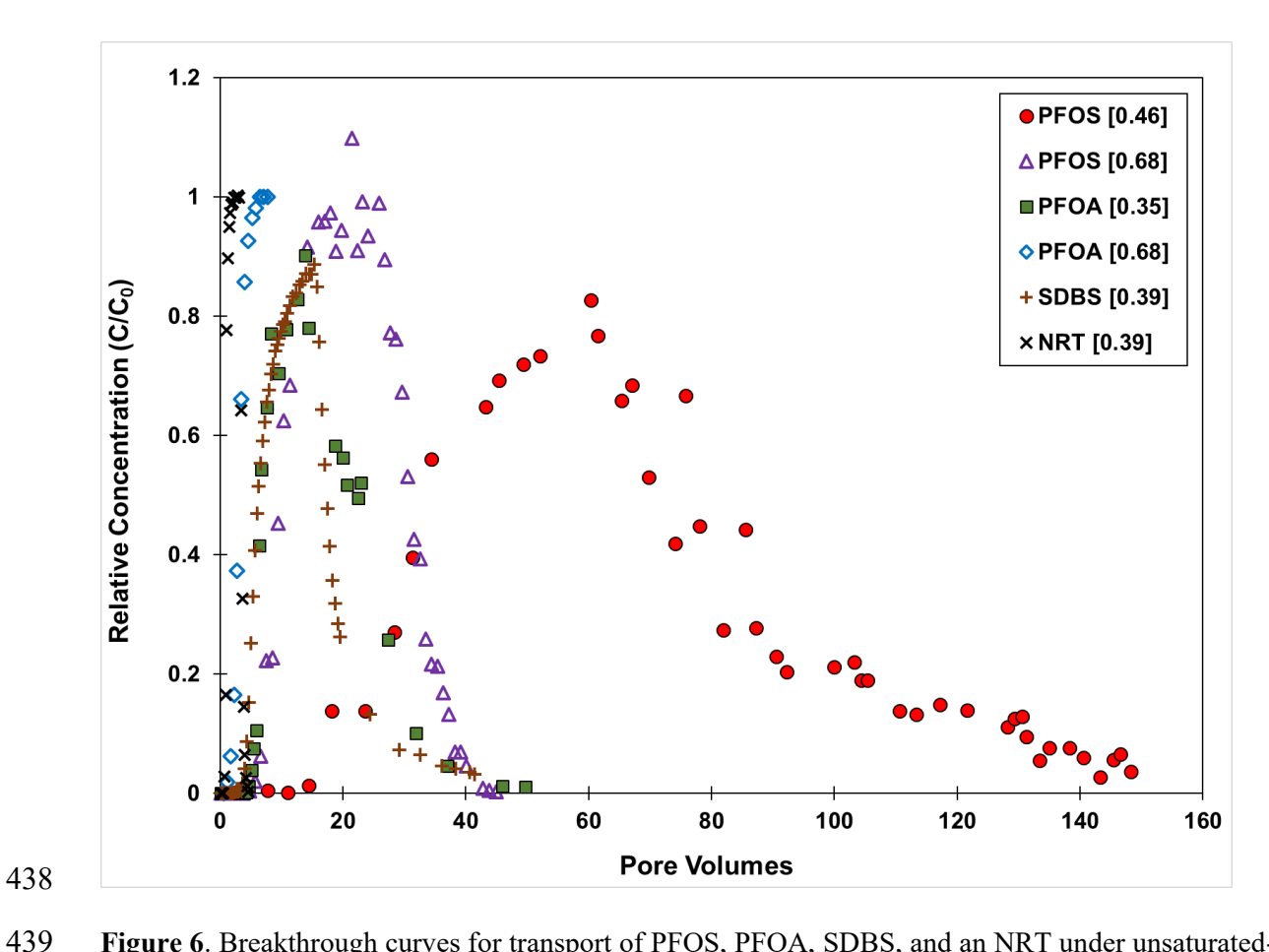


Figure 6. Breakthrough curves for transport of PFOS, PFOA, SDBS, and an NRT under unsaturated-flow conditions (water saturations are reported in the brackets).

The measured retardation factors for PFOS and PFOA are reported in Table 2. Values differ among the replicates due in part to different bulk densities and porosities of the individual column packs. The retardation factors are substantially larger for the lower water-saturation experiments for both PFOS and PFOA. They are also substantially larger for PFOS than PFOA for both sets of water saturations. Inspection of the FAWIA values shows that air-water interfacial adsorption contributes the great majority of retention, especially for PFOS. This is anticipated given the low solid-phase sorption capacity of the sand.

Retardation factors predicted for each experiment using equation (1) and independently-determined parameter values are presented in Table 2. The predicted retardation factors are similar to the measured values in all cases. The greatest deviation, ~10%, is observed for the first PFOS experiment. This magnitude of deviation is within the uncertainty range of the predicted values. The good correspondence between the predicted and measured values indicates first of all that the magnitude of retention mediating PFOS and PFOA transport at the lower water saturations was accurately represented by equation (1), and concomitantly that air-water interfacial adsorption and solid-phase sorption provided the only measurable contributions to retention. Second, the good match indicates that the values used for the input parameters to equation (1) were robust. These results are consistent with those reported in prior works for PFAS transport at higher water saturations (Lyu et al., 2018; Brusseau et al., 2021).

The arrival fronts for the NRT, SDBS, PFOS, and PFOA at lower and higher water saturations are presented in Figure 7. Note that the data are presented as relative pore volumes, wherein the eluted pore volumes are normalized by the respective retardation factors. This approach allows direct comparison of breakthrough-curve profiles irrespective of the magnitudes of retardation. The normalized arrival fronts for SDBS, PFOS, and PFOA for the higher water saturations exhibit similar profiles, and are consistent with the fronts of both NRTs. Conversely, the normalized arrival fronts for SDBS, PFOS, and PFOA for the lower water saturations exhibit a degree of early breakthrough (shifted leftward) compared to the respective fronts for the higher water saturations and to the NRT front for the lower water saturation.

A number of processes can cause early breakthrough. One process, surfactant-induced flow, can be ruled out in this case based on the results presented in section 3.1. Observations of early breakthrough for solute transport under unsaturated-flow conditions can be a result of

increased flow-path complexity and related factors, as has been observed for NRT transport in prior experiments discussed in the Introduction. However, the NRT fronts are coincident for the two saturations, indicating that the transport of the NRTs was not affected. Hence, the early breakthrough does not appear to be a result of nonideal flow phenomena. The fact that the early breakthrough is observed only for the interfacially active solutes indicates that the nonideal behavior is related to retention. In addition, the nonideal behavior is most likely related to air-water interfacial adsorption, given that it is the predominant source of retention. Nonlinear adsorption does not cause early breakthrough for favorable adsorption conditions (e.g., Freundlich exponent <1). Additionally, the early breakthrough is not observed for the higher water saturations, which were conducted with the same input concentrations. Furthermore, PFAS air-water interfacial adsorption has been demonstrated to be linear for these lower-concentration ranges (Brusseau et al., 2021). Hence, the nonideal behavior most likely accrues from a kinetic limitation. This will be assessed with the Damkohler Number analysis.

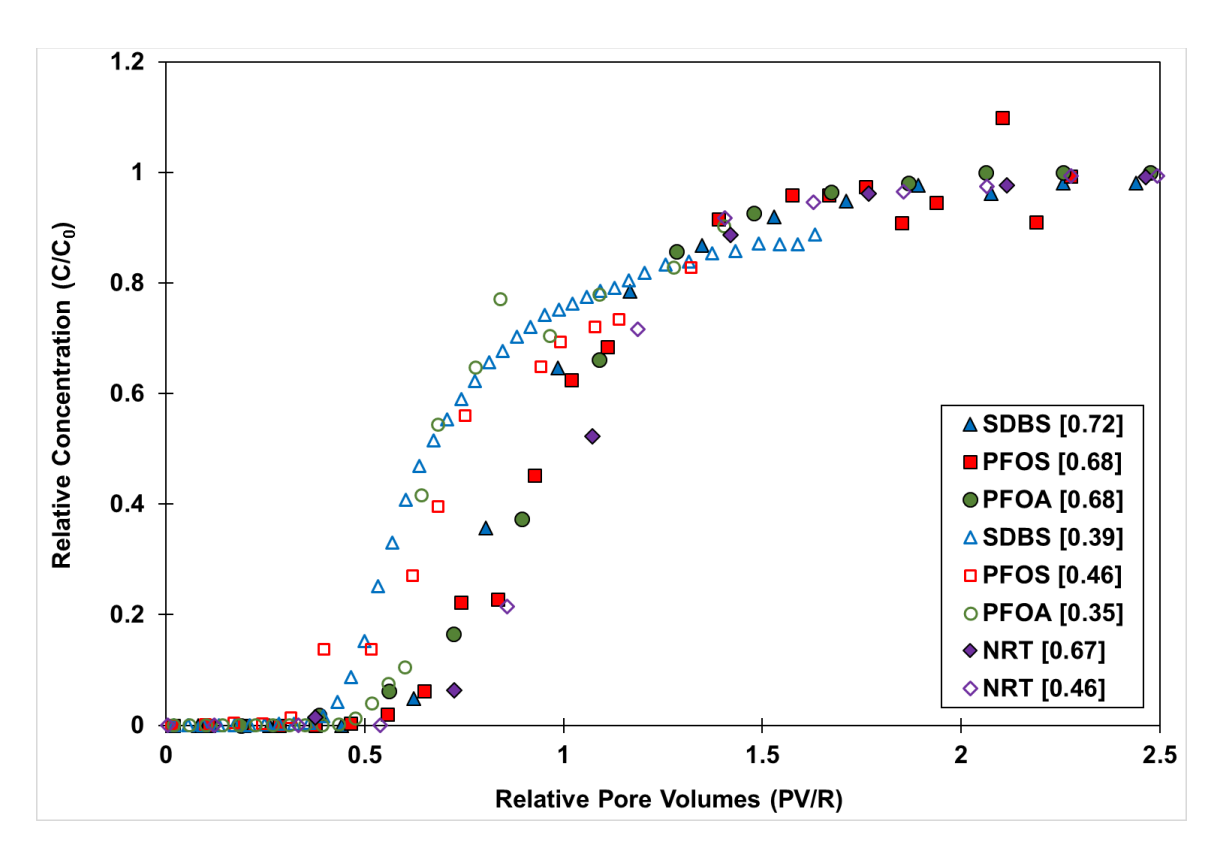


Figure 7. Breakthrough curves for transport of PFOS, PFOA, SDBS, and an NRT under unsaturated-flow conditions (water saturations are reported in the brackets). Eluted pore volumes (PV) are divided by the respective retardation factors (R).

Brusseau (2020) determined a mean ω of ~40 from an analysis of PFOA and SDBS transport at a mean water saturation of 0.75 in the same sand as used herein. Using equation (5), the ω of 40 scales to ~3 for a water saturation of 0.4, the mean of the low water-saturation experiments. Damkohler Numbers have an effective range of approximately 0.01 to 100 for transport in porous media. For ω of 100, mass transfer is sufficiently rapid compared to residence time that it can be treated as effectively instantaneous. A value of 0.01 represents the effective lower limiting case for which mass transfer is extremely rate limited with respect to transport. The ω of 40 reported in Brusseau (2020) for higher water saturations indicates that air-water interfacial adsorption was effectively instantaneous compared to the residence time. This is consistent with the fact that the breakthrough curves did not exhibit early breakthrough. Conversely, the ω of ~3

obtained for the lower water saturations indicates that air-water interfacial adsorption was likely rate limited to some degree. This would explain the early breakthrough observed for PFOS, PFOA, and SDBS in the lower water-saturation experiments. These results suggest that access to a portion of air-water interface may have been mediated by mass-transfer constraints for the lower water saturations.

The results of the Damkholer Number analysis suggest that air-water interfacial adsorption may have been impacted by mass-transfer constraints for the lower water-saturation experiments. However, the consistency between the predicted and measured retardation factors indicates that, while mass-transfer constraints or other nonideal interfacial adsorption processes may have impacted the breakthrough-curve profiles, they did not measurably impact the magnitude of adsorption. One factor contributing to the absence of impacts to the measured retardation factors is the use of moment analysis as the method of their determination. It is well established that moment analysis is in theory not affected by the impacts of mass-transfer constraints (e.g., Kucera, 1965; Valocchi, 1985). This has been demonstrated for PFAS transport in prior works. For example, sorption isotherms and K_d values measured for PFOS and PFOA with the miscible-displacement method were consistent with batch-measured equilibrium data, even though the transport of PFOS and PFOA was influenced significantly by rate-limited sorption (Brusseau et al., 2019b; Van Glubt et al., 2021).

Considering the high-resolution measurements conducted for water saturation and airwater interfacial area, any significant deviations between the predicted and measured retardation factors would reasonably be attributed to a failure to accurately represent the magnitudes of the adsorption coefficients. This assessment would be focused primarily on the K_{aw} values, given the very low contribution of solid-phase sorption. However, the consistency between the predicted

and measured retardation factors indicates that the K_{aw} values used for the predictions accurately represented the magnitude of air-water interfacial adsorption observed under transport conditions.

To further assess their representativeness, K_{aw} values can be determined from the transport experiments as described in the Materials and Methods. The mean transport-measured values are 0.036 cm⁻¹ for PFOS and 0.0026 cm⁻¹ for PFOA. These values are very close to those determined from the surface-tension measurements (PFOS-0.034, PFOA-0.0027). They are also consistent with values measured with other methods. McMurdo et al. (2008) employed an aerosol-generation method and reported an enrichment factor of 4.4 for PFOA in a filtered river-water solution, which translates to a K_{aw} of 0.0028 cm⁻¹. Reth et al. (2011) used the surface-microlayer sampling method and obtained enrichment factors of 1.7 and 15 for PFOA and PFOS, respectively, in tap water. These translate to K_{aw} values of 0.0035 cm⁻¹ for PFOA and 0.07 cm⁻¹ for PFOS. It is important to point out that the K_{aw} values measured with these three methods represent equilibrium values. These results demonstrate that the miscible-displacement method as employed herein produced accurate measurements of equilibrium-equivalent K_{aw} values, even in the presence of mass-transfer constraints.

The results of this study can be used to address the speculation concerning limitations of the miscible-displacement method for characterizing the air-water interfacial adsorption of interfacially active solutes. The good match between predicted and measured retardation factors demonstrates that the transport experiments produced robust measurements of PFAS retention and specifically air-water interfacial adsorption, both in the presence and absence of the high-resolution ancillary measurements provided by the instrumented column. This is further supported by the similarity of the transport-measured K_{aw} values to independently-measured equilibrium values. These results disprove the speculation posed by Costanza-Robinson and Henry (2017) and

Schaefer et al. (2022b) that the miscible-displacement method, at least as applied herein, produces inaccurate measurements of retention magnitude due to surfactant-induced flow, uncertainty in measuring water-saturation status, or the impact of mass-transfer constraints.

4. Conclusions

This study investigated the transport of PFOS and PFOA under relatively low water saturations in a well-characterized sand. An instrumented column was used for some experiments to provide real-time in-situ monitoring of water saturation and matric potential. Additionally, experiments were conducted wherein the nonreactive tracer was present in the PFAS solution, allowing simultaneous measurements of transport. The results showed that water saturations and matric potentials varied minimally during the experiments, indicating steady-state flow conditions. The breakthrough curves for the NRT tests conducted simultaneously with PFAS were coincident with those measured for the sequential NRT tests, indicating that the presence of PFAS had no measurable impact on solute transport and thus water flow. In addition, the flow rates exhibited minimal variation over the course of the experiments. In total, these results demonstrate that surfactant-induced flow and other non-ideal hydraulic processes did not materially impact PFAS transport for the conditions of these experiments.

Air-water interfacial adsorption was demonstrated to provide the great majority of retention for PFOS and PFOA. Retention was shown to be significantly greater for the lower water saturations, due to the larger extant air-water interfacial areas. Independently determined retention parameters were used to predict retardation factors, which were similar to the measured values in all cases. The consistency between the predicted and measured values indicates that PFAS retention was accurately represented. Furthermore, the K_{aw} values measured from the transport

experiments were consistent with values measured by three independent equilibrium-based methods, demonstrating that the miscible-displacement method produced accurate measurements of air-water interfacial adsorption.

Based on these results, it appears that the air-water interfacial adsorption processes mediating the magnitude of PFOS and PFOA retention under lower water-saturation conditions are consistent with those for higher water saturations. This provides some confidence that our understanding of PFAS retention obtained from work conducted at higher water saturations is applicable to lower water saturations. The consistency of results also suggests that the air-water interfacial adsorption process is the same for PFOS, PFOA, and SDBS, with the specific magnitude of retention a function of their respective K_{aw} values and the extant water saturation.

Declaration of Competing Interest

The authors declare that they have no known competing financial interests or personal relationships that could have appeared to influence the work reported in this paper.

Acknowledgements

This research was supported by the Hydrologic Sciences Program of the National Science Foundation (2023351) and the Environmental Security Technology Certification Program (ER21-5041 and ER23-7850). We thank Shalini Kadinappulige, Asma El Ouni, and Jack Welchert for their assistance. We also thank the reviewers and Editor for their constructive comments and suggestions.

593 References

- Abraham, J.E.F., Mumford, K.G., Patch, D.J., and Weber, K.P. (2022). Retention of PFOS and
- 595 PFOA mixtures by trapped gas bubbles in porous media. Environmental Science & Technology,
- 596 56, 15489-15498.

597

Araujo, J.B., Mainhagu, J., and Brusseau, M. L. (2015). Measuring air—water interfacial area for soils using the mass balance surfactant-tracer method. Chemosphere, 134: 199-202.

600

Biggar, J.W. and Nielsen, D.R. (1960). Diffusion effects in miscible displacement occurring in saturated and unsaturated porous materials. J. Geophys. Res., 65, 2887-2895.

603

- Bond, W.J. and Wierenga, P.J. (1990). Immobile water during solute transport in unsaturated sand columns. Water Resour. Res., 26, 2475-2481.
- 606 1990.

607

Brusseau, M.L. (2020). Simulating PFAS transport influenced by rate-limited multi-process retention. Water Res. 168, 115179.

610

- Brusseau, M. L. (2023). Determining air-water interfacial areas for the retention and transport of PFAS and other interfacially active solutes in unsaturated porous media. The Science of the Total
- 613 Environment, 884, 163730–163730.

614

Brusseau, M. L., and Guo, B. (2021). Air-water interfacial areas relevant for transport of per and poly-fluoroalkyl substances. Water Research, 207: 11778.

617

Brusseau, M.L., Guo, B. (2022). PFAS concentrations in soil versus soil porewater: Mass distributions and the impact of adsorption at air-water interfaces. Chemosphere 302,134938.

620

Brusseau, M.L., Peng, S., Schnaar, G., and Murao, A. (2007). Measuring air—water interfacial areas with X-ray microtomography and interfacial partitioning tracer tests. Environ. Sci. Technol., 41, 1956–1961.

624

Brusseau, M.L., El Ouni, A., Araujo, J. B., and Zhong, H. (2015). Novel methods for measuring air–water interfacial area in unsaturated porous media. Chemosphere, 127, 208–213.

627

Brusseau, M.L., Yan, N., Van Glubt, S., Wang, Y., Chen, W., Lyu, Y., Dungan, B., Carroll, K.C., and Holguin, F.O. (2019a). Comprehensive retention model for PFAS transport in subsurface systems. Wat. Res., 148, 41–50.

631

Brusseau, M.L., Khan, N., Wang, Y., Yan, N., Van Glubt, S., and Carroll, K.C. (2019b). Nonideal transport and extended elution tailing of PFOS in soil. Environ. Sci. Technol. 53, 10654–10664.

634

Brusseau, M.L., Anderson, R.H., Guo, B., 2020a. PFAS concentrations in soils: Bbackground levels versus contaminated sites. Sci. Total. Environ. 740 article140017.

Brusseau, M.L., Lyu, Y., Yan, N. and Guo, B., 2020b. Low-concentration tracer tests to measure air-water interfacial area in porous media. Chemo. 250, article 26305.

640

643

646

650

657

660

663

667

671

675

- Brusseau, M.L., Guo, B., Huang, D., Yan, N., and Lyu, Y. (2021). Ideal versus nonideal transport of PFAS in unsaturated porous media. Water Research, 202, 117405–117405.
- 644 Costanza-Robinson, M.S. and Brusseau, M.L. (2002). Air-water interfacial areas in unsaturated 645 soils: Evaluation of interfacial domains. Water Resour. Res., 38, 131-137.
- 647 Costanza-Robinson, M.S. and Henry, E.J. (2017). Surfactant-induced flow compromises 648 determination of air-water interfacial areas by surfactant miscible-displacement. Chemosphere 649 171, 275-283.
- De Smedt, F., and P. J. Wierenga (1984). Solute transfer through columns of glass beads, Water Resour. Res., 20, 225-232.
- 654 El Ouni, A., Guo, B., Zhong, H., and Brusseau M.L. (2021) Testing the validity of the miscible-655 displacement interfacial tracer method for measuring air-water interfacial area: Independent 656 benchmarking and mathematical modeling. Chemosphere, 263: 128193.
- EPA 2016. Definition and procedure for the determination of the method detection limit, Revision 2. Office of Water. EPA 821-R-16-006.
- Gaudet, J.P., H. Jegat, G. Vachaud, and P. J. Wierenga (1977). Solute transfer with exchange between mobile and stagnant water through unsaturated sand. Soil Sci. Soc. Am. J., 41, 665-671.
- 664 Guo, B., Zeng, J., Brusseau, M.L. (2020). A mathematical model for the release, transport, and 665 retention of per- and polyfluoroalkyl substances (PFAS) in the vadose zone. Water Resour. Res. 666 56, 21.
- Hasan, S., V. Niasar, N.K. Karadimitriou, J.R.A. Godinho, N.T. Vo, S. An, A. Rabbani, and H.
 Steeb. (2020). Direct characterization of solute transport in unsaturated porous media using fast
 X-ray synchrotron microtomography. Proc. Natl. Acad. Sci. 117, 23443.
- Huang, D., Saleem, H., Guo, B., and Brusseau, M. L. (2022). The impact of multiple-component PFAS solutions on fluid-fluid interfacial adsorption and transport of PFOS in unsaturated porous media. The Science of the Total Environment, 806, 150595–150595.
- Ji, Y., Yan, N., Brusseau, M. L., Guo, B., Zheng, X., Dai, M., Liu, H., and Li, X. (2021). Impact of a hydrocarbon surfactant on the retention and transport of perfluorooctanoic acid in saturated and unsaturated porous media. Environmental Science & Technology, 55(15), 10480–10490.
- Karagunduz, A., M.H. Young, and K.D. Pennell (2015). Influence of surfactants on unsaturated water flow and solute transport, Water Resour. Res., 51, 1977–1988.

- Kim, H., Rao, P.S.C., Annable, M.D. (1997). Determination of effective air-water interfacial area
- in partially saturated porous media using surfactant adsorption. Water Resour. Res. 33, 2705–2711.

- Krupp, H.K. and Elrick, D.E. (1968). Miscible Displacement in an unsaturated glass bead medium.
- 687 Water Resour. Res., 4, 809-815.

688

Kucera, E. (1965). Contribution to the theory of chromatography linear non-equilibrium elution chromatography. J. Chromatogr., 19, 237–248.

691

Kumahor, S.K., de Rooij, G.H., Schlüter, S., Vogel, H.-J., 2015. Water flow and solute transport in unsaturated sand—A comprehensive experimental approach. Vadose Zone J. 14, 1-9.

694

Lenhart, J. J., and J. E. Saiers (2002). Transport of silica colloids through unsaturated porous media: Experimental results and model comparisons, Environ. Sci. Technol., 36, 769–777.

697

698 Li, Z., Lyu, X., Gao, B., Xu, H., Wu, J., and Sun, Y. (2021). Effects of ionic strength and cation 699 type on the transport of perfluorooctanoic acid (PFOA) in unsaturated sand porous media. Journal 700 of Hazardous Materials, 403, 123688–123688.

701

Lyu, X., Liu, X., Sun, Y., Gao, B., Ji, R., Wu, J., & Xue, Y. (2020). Importance of surface roughness on perfluorooctanoic acid (PFOA) transport in unsaturated porous media. Environmental Pollution, 266, 115343–115343.

705

Lyu, X., Li, Z., Wang, D., Zhang, Q., Gao, B., Sun, Y., and Wu, J. (2022b). Transport of perfluorooctanoic acid in unsaturated porous media mediated by SDBS. Journal of Hydrology, 607, 127479.

709

Lyu, Y. and Brusseau, M. L. (2020). The influence of solution chemistry on air-water interfacial adsorption and transport of PFOA in unsaturated porous media. The Science of the Total Environment, 713, 136744–136744.

713

Lyu, Y., Brusseau, M. L., Chen, W., Yan, N., Fu, X., and Lin, X. (2018). Adsorption of PFOA at the Air–Water Interface during Transport in Unsaturated Porous Media. Environmental Science & Technology, 52(14), 7745–7753.

717

Lyu, Y., Wang, B., Du, X., Guo, B., and Brusseau, M.L. (2022a). Air-water interfacial adsorption of C4-C10 perfluorocarboxylic acids during transport in unsaturated porous media. The Science of the Total Environment, 831, 154905–154905.

721

- MacLean, B., Tomazela, D.M., Shulman, N., Chambers, M., Finney, G.L., Frewen, B., Kern, R.,
- 723 Tabb, D.L., Liebler, D.C. and MacCoss, M.J. (2010). Skyline: an open source document editor
- for creating and analyzing targeted proteomics experiments. Bioinformatics 26, 966-968.

- McMurdo, C.J., Ellis, D.A., Webster, E., Butler, J., Christensen, R.D., Reid, L.K. (2008). Aerosol
- enrichment of the surfactant PFO and mediation of the water-air transport of gaseous PFOA.
- 728 Environ. Sci. Technol. 42, 3969–3974.

730 Millington, R.J., and J.P. Quirk (1961). Permeability of porous solids, Trans. Faraday Soc., 57, 1200-1207.

732

Padilla, I.Y., Yeh, T.C.J., and Conklin, M.H. (1999). The effect of water content on solute transport in unsaturated porous media. Water Resour. Res., 35, 3303-3313.

735

Rankin, K., Mabury, S., Jenkins, T., Washington, J. (2016). A North American and global survey of perfluoroalkyl substances in surface soils: distribution patterns and mode of occurrence. Chemosphere 161, 333–341.

739

Raoof, A. and S. Hassanizadeh (2013). Saturation-dependent solute dispersivity in porous media: pore-scale processes. Water Resour. Res. 49, 1943–1951.

742

Reth, M., Berger, U., Broman, D., Cousins, I.T., Nilsson, E.D., McLachlan, M.S. (2011). Water-to-air transfer of perfluorinated carboxylates and sulfonates in a sea spray simulator. Environ. Chem. 8, 381–388.

746

Rimon, Y., O. Dahan, R. Nativ, and S. Geyer. 2007. Water percolation through the deep vadose zone and groundwater recharge: Preliminary results based on a new vadose zone monitoring system. Water Resour. Res., 43, 1–12.

750

Schaefer, C.E., Lavorgna, G.M., Lippincott, D.R., Nguyen, D., Christie, E., Shea, S., O'Hare, S.,
 Lemes, M.C.S., Higgins, C.P., and Field, J. (2022a). A field study to assess the role of air-water
 interfacial sorption on PFAS leaching in an AFFF source area. J. Contam. Hydrol. 248, 104001.

754

Schaefer, C.E., Nguyen, D., Meng, P., Fang, Y., and Knappe, D.R.U. (2022b). Sorption of perfluoroalkyl ether carboxylic acids (PFECAs) at the air-water interface in porous media: Modeling perspectives. J. Hazard. Mater. Adv., 6, 100062.

758

Smith, J.E. and Gillham, R.W. (1999). Effects of solute concentration-dependent surface tension on unsaturated flow: Laboratory sand column experiments. Water Resour. Res., 35, 973-982.

761

Toride, N., M. Inoue, and F.J. Leij (2003), Hydrodynamic dispersion in an unsaturated dune sand, Soil Sci. Soc. Am. J., 67, 703–712.

764

Turkeltaub, T., Dahan, O., and Kurtzman, D. (2014). Investigation of groundwater recharge under agricultural fields using transient deep vadose zone data. Vadose Zone J., 13, 1-13.

767

Valocchi, A.J. (1985). Validity of the local equilibrium assumption for modeling sorbing solute transport through homogeneous soil. Water Resour. Res., 21, 808–820.

770

Van Glubt, S., Brusseau, M. L., Yan, N., Huang, D., Khan, N., and Carroll, K. C. (2021). Column versus batch methods for measuring PFOS and PFOA sorption to geomedia. Environmental Pollution, 268, 115917–115917.

- Washington, J., Rankin, K., Libelo, E., Lynch, D., Cyterski, M. (2019). Determining global
- background soil PFAS loads and the fluorotelomer-based polymer degradation rates
- that can account for these loads. Sci. Total Environ. 651, 2444–2449.

Yan, N., Ji, Y., Zhang, B., Zheng, X., and Brusseau, M.L., 2020. Transport of GenX in Saturated and Unsaturated Porous Media. Environmental Science & Technology, 54, 11876-11885.

781

Yao, T., Wierenga, P.J., Graham, A.R., and Neuman, S.P. (2004). Neutron probe calibration in a vertically stratified vadose zone. Vadose Zone J., 3, 1400–1406.

- Zhuang, L., A. Raoof, M.G. Mahmoodlu, S. Biekart, R. de Witte, L. Badi, M.T. van Genuchten,
- 786 K. Lin, (2021). Unsaturated flow effects on solute transport in porous media. J. Hydrol. 598,
- 787 126301.